

PAPER

[View Article Online](#)
[View Journal](#) | [View Issue](#)Cite this: *Dalton Trans.*, 2025, **54**, 11306Amino-functionalized cerium based MOF for sustainable CO₂ fixation into cyclic carbonates†Yogesh Kumar, ^a Rishukumar Panday ^b and Shaibal Banerjee ^{*a}

The conversion of CO₂ into valuable chemicals is a pivotal strategy to mitigate environmental and energy challenges. In this context, we report the design and synthesis of a cerium-based metal–organic framework {[Ce(L-NH₂)_{0.5}(NO₃)(H₂O)₂]·2DMF} (**Ce-TPTC-NH₂**), constructed from Ce(III) centers and a precisely engineered amino-functionalized terphenyl tetracarboxylate ligand {L-NH₂} (TPTC-NH₂). This crystalline, microporous framework not only exhibits excellent catalytic performance in the solvent-free cycloaddition of CO₂ with suitable epoxides, achieving >99% conversion under mild conditions (5 bar CO₂, 100 °C, 0.06 mol% catalyst) but also demonstrates unprecedented structural stability and reusability over multiple cycles. The synergistic interplay between Lewis acidic Ce³⁺ centers and basic –NH₂ groups enables enhanced activation of both CO₂ and epoxide substrates while lowering the activation barrier. Importantly, this Ce-MOF integrates bifunctional acid–base sites and is tailored specifically for CO₂ fixation. The catalyst retained its crystallinity and >90% activity after five cycles, confirming its practical viability. This work introduces a design pathway for amine-functionalized Ce-MOFs, showcasing their potential as highly efficient, stable, and reusable heterogeneous catalysts for CO₂ fixation under solvent-free conditions.

Received 6th April 2025,
Accepted 30th June 2025

DOI: 10.1039/d5dt00825e

rsc.li/dalton

Introduction

The atmospheric CO₂ levels have significantly increased since the Industrial Revolution, leading to major environmental challenges.¹ While CO₂ is essential for regulating Earth's temperature, its excessive emissions are driving climate change, highlighting the need for effective capture and utilization strategies. One promising approach is the catalytic conversion of CO₂ into value-added chemicals, such as cyclic carbonates, which are widely used in the polymer and pharmaceutical industries. The cycloaddition of CO₂ with epoxides offers a clean and practical route for converting exhaust carbon into useful chemicals, supporting the global pursuit of net-zero emissions. However, activating CO₂ transformation presents a significant challenge due to the high bond enthalpy of the C=O bond (+805 kJ mol^{−1}), making the choice of catalysts crucial for improving both the efficiency and scalability of the process.² Heterogeneous catalysts, including zeolitic imidazolate frameworks,³ and transition-metal complexes^{4,5} have been

explored for CO₂ conversion, but their low catalytic stability, poor recyclability, and dependence on harsh reaction conditions (high temperature and high CO₂ pressure) limit their practical application. Additionally, these active sites often require high CO₂ loading, which can lead to reduced conversion efficiency and selectivity. Among the advanced materials, metal–organic frameworks (MOFs) have emerged as promising candidates for CO₂ adsorption.^{6–8} Due to their high surface area, tunable porosity, and functionalizing ability, MOFs offer a unique platform for heterogeneous catalysis, as their structures can be tailored to incorporate catalytically active sites.^{1,9,10} In particular, zirconium-based MOFs have demonstrated excellent stability; however, their synthesis typically requires high temperature and pressure, making large-scale production challenging.^{11,12}

Recent research focus has shifted towards lanthanide-based MOFs, particularly cerium, for catalytic applications, primarily due to their large size and high coordination numbers. These frameworks exhibit excellent adsorption capacity, versatile redox behavior, and water stability. The latter arises from the highly acidic lanthanide centers that form strong coordination bonds with multidentate organic linkers, enhancing both the structural rigidity and the hydrophobic character of the material. Furthermore, the phenomenon of lanthanide contraction, arising from the poor shielding of the 4f orbitals, results in a gradual decrease in ionic radii across the series, leading to a higher effective nuclear charge. This increased

^aDepartment of Applied Chemistry, Defence Institute of Advanced Technology (DIAT), Pune 411025, India. E-mail: banerjeess@diat.ac.in^bDepartment of Chemistry, Indian Institute of Science Education and Research, Pune, Dr. Homi Bhabha Road, Pashan, Pune – 411008, India† Electronic supplementary information (ESI) available. CCDC 2429809. For ESI and crystallographic data in CIF or other electronic format see DOI: <https://doi.org/10.1039/d5dt00825e>

Lewis acidity enhances the metal centres' ability to coordinate with electron-rich substrates such as epoxides, thereby facilitating efficient catalytic activation. Cerium-MOFs are mostly favored due to their abundance, cost-effectiveness, and redox-active $\text{Ce}^{3+}/\text{Ce}^{4+}$ centers.^{13–16} Unlike Zr-MOFs, Ce-MOFs can be synthesized under milder conditions while maintaining comparable catalytic activity and stability. These materials have been extensively studied in applications such as gas storage, energy conversion, and photocatalysis.^{17–21} Recently, Ma *et al.* have synthesized lanthanide-based MOFs using cerium metal ions.²² This MOF facilitates the removal of fluoride from water by adsorption. In another study, Lammert *et al.* have synthesized a series of Cerium-based MOFs, including various linker chains.²³ The produced MOFs have significant thermal stability and can serve as catalysts in many chemical conversions, including alcohol oxidation.²³ However, their potential in CO_2 conversion remains relatively underexplored.^{24–26}

The design and synthesis of porous materials with well-defined functionalities remain a cornerstone of materials chemistry, particularly in the context of CO_2 capture and conversion. In this work, we report the synthesis of a novel cerium-based metal-organic framework $\{[\text{Ce}(\text{L-NH}_2)_{0.5}(\text{NO}_3)(\text{H}_2\text{O})_2]\cdot 2\text{DMF}\}$ (**Ce-TPTC-NH₂**), constructed from an amine-functionalized *p*-terphenyl-3,5,3',5'-tetracarboxylate $\{\text{L-NH}_2\}$ (TPTC-NH₂) ligand. The synthesis yields a highly crystalline and stable framework, as confirmed by single-crystal X-ray diffraction (SCXRD). Further, microscopic analysis using high-resolution transmission electron spectroscopy (HR-TEM), X-ray photoelectron spectroscopy (XPS), field-emission scanning electron microscopy (FE-SEM), and temperature-programmed desorption (TPD) establishes its composition, porosity, morphology, and CO_2 adsorption capacity. To enhance catalytic efficiency, amine ($-\text{NH}_2$) functionalization was introduced, as NH_2 groups act as Lewis-basic sites, facilitating CO_2 interactions and improving electronic properties. **Ce-TPTC-NH₂** features a π -conjugated terphenyl core that enhances framework stability and electronic interactions, while the amine ($-\text{NH}_2$) moieties facilitate strong acid-base interactions, improving CO_2 affinity and catalytic efficiency;^{27–30} Cerium was selected as the metal center due to its redox-active nature ($\text{Ce}^{3+}/\text{Ce}^{4+}$), high Lewis acidity, and strong affinity for oxygen-donor ligands. Additionally, the strong coordination between the highly charged Ce^{3+} ions and the tetra carboxylate TPTC ligand imparts hydrophobic character to the framework, enhancing its resistance to hydrolysis. The coexistence of Lewis-acidic Ce metal sites and basic amine groups creates a synergistic effect, enabling efficient CO_2 activation and conversion.^{31–33}

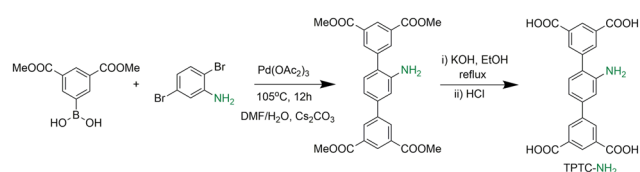
The catalytic efficiency of **Ce-TPTC-NH₂** is demonstrated in the solvent-free cycloaddition of CO_2 with epoxides, achieving >99% conversion. Moreover, **Ce-TPTC-NH₂** exhibits good recyclability, retaining its catalytic activity over five consecutive cycles without significant degradation. Compared to previously reported Ce-MOFs, **Ce-TPTC-NH₂** exhibits superior CO_2 affinity and catalytic efficiency, establishing it as a highly effective and reusable platform for sustainable CO_2 utilization.³⁴

Results and discussion

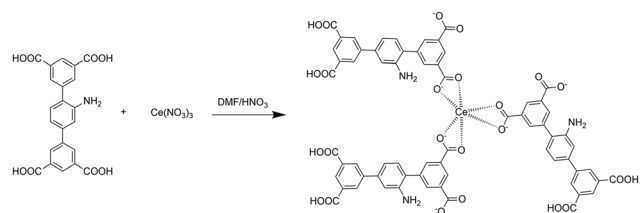
The **Ce-TPTC-NH₂** MOF was synthesized by the solvothermal reaction of TPTC-NH₂ ligand and $\text{Ce}(\text{NO}_3)_3\cdot 6\text{H}_2\text{O}$ in dimethyl formamide (DMF) solvent. The TPTC-NH₂ ligand was synthesized with modifications to previously reported procedures (Schemes 1 and 2).³⁵

In order to understand the synergistic effect of **Ce-TPTC-NH₂** catalyst for CO_2 capture and conversion. First, the structural and electronic properties of **Ce-TPTC-NH₂** MOF were systematically analyzed through various spectroscopic techniques to elucidate the role of amino functionalization in optimizing these functionalities.

Single-crystal X-ray diffraction analysis revealed that **Ce-TPTC-NH₂** crystallizes in the monoclinic system with a $C2/c$ space group. The asymmetric unit shown in Fig. 1a consists of one crystallographic unit $\text{Ce}(\text{III})$ atom, a symmetrically half-unit of the TPTC-NH₂ ligand, where the $-\text{NH}_2$ group is disordered over two positions, one NO_3^- anion, two coordinated water molecules, and two free DMF molecules. A detailed examination of the coordination environment indicates that **Ce-TPTC-NH₂** forms dinuclear Ce_2 clusters, in which pairs of $\text{Ce}(\text{III})$ ions are bridged by four carboxylate groups from four distinct TPTC-NH₂ ligands (Fig. 1b). The coordination sphere of the $\text{Ce}(\text{III})$ ions is completed by disordered nitrate ions and two coordinated water molecules. The TPTC-NH₂ ligands, in turn, connect to four separate Ce_2 dimers. The overall 3D network can be simplified by considering both the Ce_2 dimers and TPTC-NH₂ ligands as 4-connecting nodes (Fig. 1c). The powder X-ray diffraction (PXRD) patterns of the simulated and as-synthesized **Ce-TPTC-NH₂** exhibit strong correspondence, signifying its phase purity. The PXRD pattern of the **Ce-TPTC-NH₂** samples is shown in Fig. 1d, displaying significant diffraction peaks at roughly 2θ values of 7.08° , 8.95° , 9.80° , and 17.51° , corresponding to the (200), (004), (112), and (204) planes,



Scheme 1 Synthetic pathway of TPTC-NH₂ by Suzuki coupling reaction.



Scheme 2 Synthetic pathway of **Ce-TPTC-NH₂**.

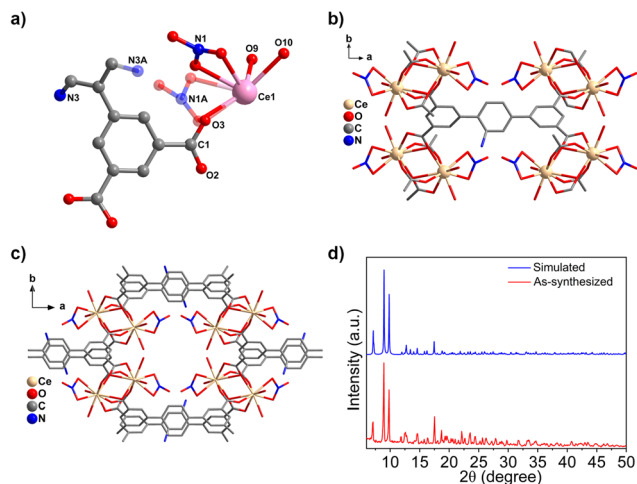


Fig. 1 (a) The asymmetric unit of **Ce-TPTC-NH₂** MOF. (b) The second building unit for the dinuclear Ce₂ cluster. (c) Packing along the *c*-axis, (d) PXRD pattern of the synthesized **Ce-TPTC-NH₂** MOF in comparison to the simulated pattern.

respectively. The XRD patterns of all samples demonstrate a significant degree of crystallinity. Furthermore, the crystallite sizes of the samples were ~ 55 nm on average, which was calculated using the main XRD peaks and the Scherrer equation *via* Xpert High Score-Plus software⁶⁴.

$$D = (K\lambda)/(\beta \cos \theta)$$

D is the average size of crystallites, K is the shape factor, λ is X-ray wavelength, β is full width at half maximum (FWHM) of the diffraction peak in radian, and θ is Bragg angle.

Field Emission Scanning Electron Microscopy (FE-SEM) was employed to observe the morphology of the synthesized crystals of **Ce-TPTC-NH₂**. In Fig. 2a, the image of **Ce-TPTC-NH₂** reveals a cluster of thick and pillared layered crystals with a size of 1–2 μm . Besides, the detailed analysis of energy-dispersive X-ray spectroscopic (EDS) results in Fig. 2b confirms the presence of Ce, O, C, and N within the synthesized compound. **Ce-TPTC-NH₂** had an optimal cerium content (16.42%), as shown in Fig. 2c, which is consistent with other reported cerium-based MOFs.²²

To further explore the coordination interaction between all the elements, present in the **Ce-TPTC-NH₂**, the XPS analysis results are presented in Fig. 3a–c. The XPS spectra of Ce(III) 3d_{5/2} and 3d_{3/2} regions for **Ce-TPTC-NH₂** are deconvoluted into four components, attributed to the formation of Ce(III) oxocluster, appearing between 882 and 904 eV (Fig. 3a). The high-resolution O 1s spectra exhibit peaks at 532.18 eV, attributed to hydroxyl bonding to metal (M–OH), and another peak at 533.58 eV, assigned to metal oxide (M–O) (Fig. 3b). This slight shift of C=O at 533 eV indicates the bonding of oxygen with cerium metal ions. The N 1s spectrum shows peaks at 400.57 eV, corresponding to the free (–NH₂) amine peak, whereas the peak at 403.08 and 407.38 eV corresponds to N–C=O of DMF bound to cerium metal ion, and nitrate ions from nitric acid,

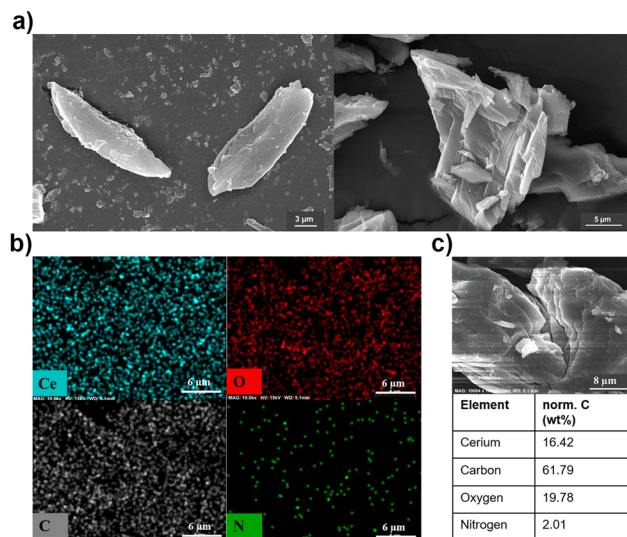


Fig. 2 (a) FE-SEM images, (b) elemental mapping, and (c) SEM-EDX elemental analyses of **Ce-TPTC-NH₂** MOF.

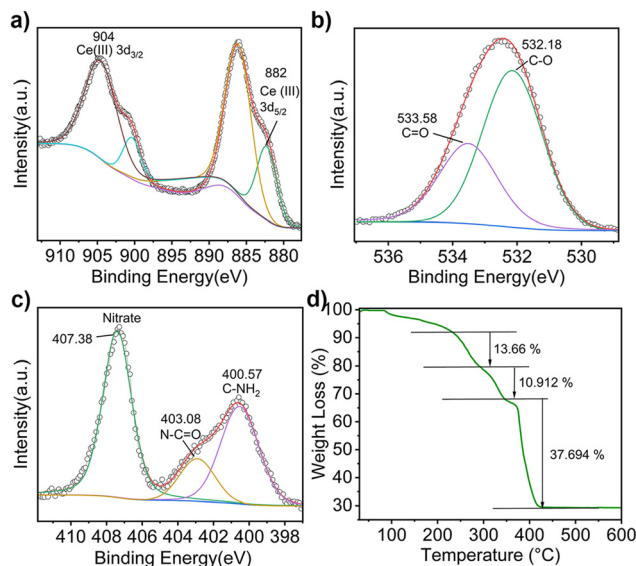


Fig. 3 XPS deconvolution spectra of the (a–c) Ce 3d, O 1s, and N 1s (d) TGA analysis of **Ce-TPTC-NH₂** MOF.

respectively. The shift in the binding energy of N–C=O and nitrate ions towards higher energy can be attributed to electronic conjugation within the framework following MOF synthesis (Fig. 3c). The C 1s spectrum has peaks at 284.94, 286.44, and 288.70 eV, corresponding to C–C, C–O–C, and O–C=O, respectively (Fig. S4†). The analysis of the peak integrations from the XPS spectrum indicates that the atomic fractions of O 1s, Ce 3d_{5/2}, C 1s, and N 1s in **Ce-TPTC-NH₂** are 33, 2.74, 55.75, and 8.51%, respectively.

To evaluate the thermal stability of **Ce-TPTC-NH₂**, thermogravimetric analysis (TGA) measurement was performed as shown in Fig. 3d. Thermogravimetric analysis of Ce-MOF

shows the initial weight loss before 200 °C should be associated with water molecules coordinated with the MOF. The weight loss in temperature ranging from 200 °C to 300 °C should be attributed to the decomposition of coordinated DMF molecules.³⁵ A substantial % weight loss of 37% appeared in the temperature range of 380–420 °C, suggesting the collapse of the frameworks and decomposition of the organic ligands. Furthermore, TGA validated the thermal robustness of **Ce-TPTC-NH₂** up to 380 °C. The BET surface area of the **Ce-TPTC-NH₂** MOF was measured and found to be similar to that of a previously reported europium-based MOF (Fig. S5†).

The strength and distribution of acidic and basic sites that facilitate reactant activation on synthesized materials were evaluated using NH₃-TPD (TPD = temperature-programmed desorption) and CO₂-TPD,³⁶ respectively, as seen in Fig. 4. The sample exhibited a desorption pattern between 100 °C and 700 °C. Acidic and basic sites in a catalyst are often categorized as weak (100–250 °C), moderate (250–450 °C), and strong (>450 °C). These peaks result from the distinct physical and chemical adsorption of CO₂ and NH₃.

The intense peak at about 300 °C in CO₂-TPD is linked to the existence of free amine sites, highlighting the impact of the (–NH₂) moiety inserted in the ligand (Fig. 4a). Simultaneously, the NH₃-TPD profile is seen in Fig. 4b. Adsorption of NH₃ at Ce-sites has been suggested to give rise to the intense desorption peak observed at 250–350 °C.³⁷ The graph demonstrates that the amine-functionalized **Ce-TPTC-NH₂** MOF possesses strong basic sites (0.940 mmol g^{–1}) and acidic sites (0.956 mmol g^{–1}), facilitating the activation of the epoxide ring and CO₂ molecule (Table 1). The synergistic effect of Lewis acidic Ce(III) sites and basic amine (–NH₂) functionalities through TPD studies, highlighting their role in CO₂ activation.

The stability of **Ce-TPTC-NH₂** was also observed in a series of solvents such as DMF, di-methyl sulfoxide (DMSO), methanol, ethanol, tetrahydrofuran (THF), boiling water, and DI water for 24 h. To further assess its chemical robustness, the MOF was soaked in mildly acidic (pH 5) and basic (pH 9) aqueous solutions. Meanwhile, the post-PXRD patterns of **Ce-TPTC-NH₂** remained almost the same as those of the as-synthesized **Ce-TPTC-NH₂**, with a slight reduction in intensities confirming its stability (Fig. S6†).^{24,25} Contact angle measure-

Table 1 Basic and acidic sites of **Ce-TPTC-NH₂** determined by CO₂ and NH₃ temperature-programmed desorption

Property	Ce-TPTC-NH₂
Weak basic sites (<250 °C)	0.265 mmol g ^{–1} (250 °C)
Moderate basic sites (250–450 °C)	1.009 mmol g ^{–1} (300 °C)
Strong basic sites (>450 °C)	0.940 mmol g ^{–1} (600 °C)
Total basic sites	2.214 mmol g ^{–1}
Weak acidic sites (<250 °C)	0.236 mmol g ^{–1} (240 °C)
Moderate acidic sites (250–450 °C)	1.077 mmol g ^{–1} (300 °C)
Strong acidic sites (>450 °C)	0.956 mmol g ^{–1} (600 °C)
Total acidic sites	2.269 mmol g ^{–1}

ment also supported the stability of **Ce-TPTC-NH₂** MOF in polar solvents (Fig. S7†).

Catalytic activity: cycloaddition reaction of epoxide with CO₂

Following activation, **Ce-TPTC-NH₂** was evaluated as a heterogeneous Lewis acid–base catalyst for the CO₂ with epoxide cycloaddition reaction. Its catalytic efficiency was systematically investigated through a series of experiments. 1-Chloro-2,3-epoxy propane (epichlorohydrin) was selected as the primary epoxide system in the coupling reaction with CO₂ under solvent-free conditions. A controlled experiment without a catalyst showed negligible conversion at 5 bar CO₂ even after 24 hours. A series of experiments using **Ce-TPTC-NH₂** MOF as a catalyst demonstrated significantly enhanced performance, achieving 99.9% selectivity for cyclic carbonates in CO₂ conversion with good yield. NMR monitoring revealed that most conversions occurred within 12 hours, with no significant progress afterward.

We further investigated the reaction conditions by modifying parameters such as catalyst dosage, temperature, and duration, as shown in Fig. 5 and Table 2. A 10 mg (~0.0168 mol% of Ce) catalyst loading achieved ~98% epoxide

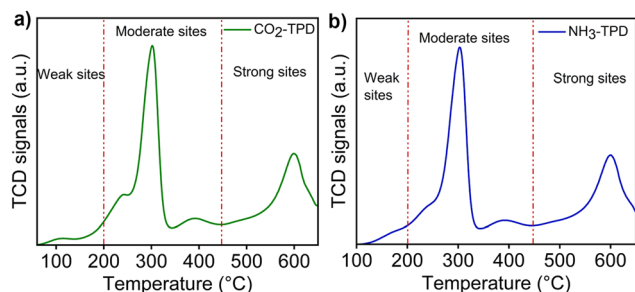


Fig. 4 Temperature-programmed desorption (TPD) (a) CO₂ and (b) NH₃ of **Ce-TPTC-NH₂** MOF.

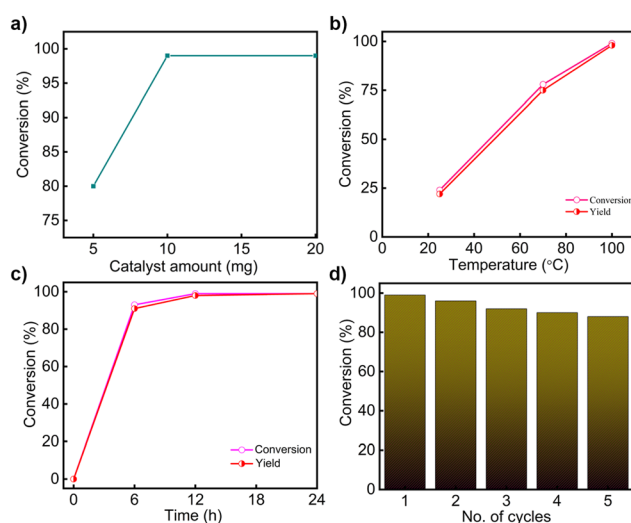
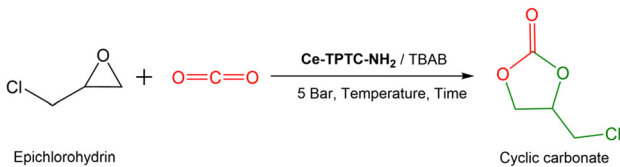


Fig. 5 Catalytic conversion of CO₂ by varying (a) catalyst amount, (b) temperature, (c) time, and (d) reusability study of catalytic conversion of CO₂ by **Ce-TPTC-NH₂** MOF.

Table 2 Catalytic activity of **Ce-TPTC-NH₂** for the cycloaddition reaction of CO₂ to cyclic carbonate


where, TBAB = *t*-butylammonium bromide

Entry	Ce-TPTC-NH₂ / TBAB ratio	Temp. (°C)	Time (h)	Conversion (%)	Yield (%)
1	0/0	100	24	10	3
2	20/0	100	24	40	17
3	0/16	100	24	23	16
4	20/16	100	12	99	99
5	10/16	100	24	99	99
6	10/16	100	12	99	98
7	20/16	70	12	84	82
8	20/16	70	24	86	83
9	10/16	70	12	78	75
10	10/16	70	24	80	73
11	20/16	rt	24	24	22
12	10/16	rt	24	18	17

Ce-TPTC-NH₂ (10 mg), TBAB (16 mg), epoxide (2 mL), CO₂ pressure (5 bar), temperature (100 °C), Time (12 h).

conversion to cyclic carbonate within 12 hours at 100 °C. Given the high yield, this loading was chosen for further optimization. The catalytic reaction was monitored using the ¹H-NMR spectrum, with the disappearance of the characteristic signal of epichlorohydrin at 3.2 ppm and the appearance of a signal at 4.9 ppm for cyclic carbonate (Fig. S8†). This analysis confirms that **Ce-TPTC-NH₂** is an efficient catalyst for CO₂-to-epichlorohydrin coupling, achieving 99.9% selectivity. Since temperature plays a crucial role in the catalytic process, lowering the reaction temperature from 100 °C to 70 °C reduces the product yield from 98% to 75%, likely due to the enhanced CO₂ incorporation into the C–O bond of oxidized epichlorohydrin at higher temperatures (Table 2). Given that CO₂ cycloaddition is exothermic, the optimal reaction temperature for **Ce-TPTC-NH₂** MOF-catalyzed CO₂ cycloaddition is determined to be 100 °C, underscoring its high catalytic efficiency.

The cycloaddition procedure yielded 97% of 4-(chloromethyl)-1,3-dioxolan-2-one product utilizing 80% CO₂. **Ce-TPTC-NH₂** as a catalyst facilitates the cycloaddition of CO₂ and epoxides through a cooperative Lewis acid–base mechanism. The Ce³⁺ centers activate the epoxide *via* coordination with its oxygen atom, while the Br[−] anion from TBAB acts as a nucleophile to promote ring opening. The enhanced catalytic activity of **Ce-TPTC-NH₂** MOF with co-catalyst tetra-butyl ammonium bromide (TBAB) arises from the synergistic interaction between cerium Lewis acidic sites and basic bromine functionality. To investigate the influence of the nucleophile on catalytic performance, three co-catalyst systems: tetrabutylammonium bromide (TBAB), chloride (TBAC), and iodide (TBAI), in the presence of the **Ce-TPTC-NH₂** catalyst, were compared. Although the Br[−] anion is moderately nucleophilic, it resulted in the highest conversion (98%), outperforming even the more nucleophilic I[−] (68%) and Br[−] system (17%).²⁵ Br[−] offers an optimal balance between nucleophilicity and leaving group ability, making it more effective than Cl[−] or I[−] in similar systems. A control reaction without TBAB resulted in a significantly lower conversion (~17%), confirming its essential role. Given its mechanistic compatibility, stability, and literature precedence, TBAB was found to be the most appropriate co-catalyst for this system.

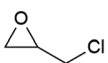
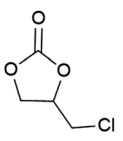

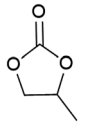
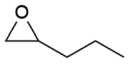
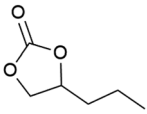
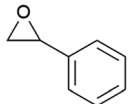
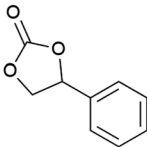
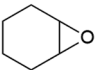
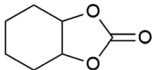
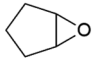
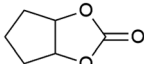
To further validate the role of basic sites in catalysis, we synthesized {[Ce(L)_{0.5}(NO₃)(H₂O)₂]}·2DMF (**Ce-TPTC**) following a previously reported procedure (Fig. S9†).²² As anticipated, **Ce-TPTC**, when used as a catalyst in combination with the co-catalyst TBAB, yielded a lower product conversion of approximately 65% with epichlorohydrin under the same reaction conditions employed for **Ce-TPTC-NH₂**. Once the optimum reaction conditions (5 atm CO₂, 12 h, 100 °C) were achieved for epichlorohydrin-to-cyclic carbonate conversion, we further tested the catalytic performance of **Ce-TPTC-NH₂** with a variety of epoxide substrates, including 2-methyloxirane, 2-propyloxirane, and 2-phenyloxirane, ranging from aliphatic to aromatic substituents.

The conversion and yield decrease as the epoxide substituent size increases, likely due to steric hindrance and electronic effects.²⁵ Bulkier epoxides with longer chains can obstruct the pores of **Ce-TPTC-NH₂**, slowing down reactant diffusion and reducing efficiency. Selectivity for the cyclic carbonate products was >99% in all instances. All cyclic carbonate products

Table 3 Comparison of **Ce-TPTC-NH₂** with other heterogeneous catalysts in the cycloaddition of CO₂ to cyclic carbonate

Material	Dosage	Pressure	Temperature	Co-catalyst	Cycles	Conversion	Ref.
MIL-101(Cr)-IP	42 mg	0.8 MPa	50 °C	—	—	91%	38
HPC-800	30 mg	0.15 bar	RT	TBAB	3	90%	39
PNU-25-NH ₂ /TBAB	1 mol%	1 bar	55 °C	TBAB	4	92%	26
NH ₂ -Ce-MUM-2	20 mg	1 atm	50 °C	TBAB	6	93%	24
Gd-TPTC-NH-[BMIM]Br	20 mg	0.1 MPa	100 °C	TBAB	5	91%	40
Zr(H ₄ L)	0.1 mmol	9.8 atm	100 °C	TBAB	5	>99%	41
Ce ₂ NDC ₃	15 mg	0.1 MPa	RT	TBAB	5	89%	42
Ce(HTCPB)	0.0145 mmol	10 bar	100 °C	TBAB	3	97%	43
Meim-UiO-66	50 mg	0.1 MPa	120 °C	—	6	46%	44
Gd-TPTC-NH ₂	20 mg	0.1 MPa	100 °C	TBAB	—	31%	40
Ce-TPTC-NH₂	20 mg	5 atm	100 °C	TBAB	5	>99%	This work

Table 4 Synthesis of cyclic carbonates from CO₂ and epoxides catalysed by **Ce-TPTC-NH₂**

Sr. no.	Epoxide substrate	Product	Structure Type	Time (h)	Conversion (%)	Yield (%)
1	 2-(chloromethyl)oxirane	 4-(chloromethyl)-1,3-dioxolan-2-one	Aliphatic terminal	12	99%	98%
2	 2-methyloxirane	 4-(methyl)-1,3-dioxolan-2-one	Aliphatic terminal	12	93%	89%
3	 2-propyloxirane	 4-(propyl)-1,3-dioxolan-2-one	Linear aliphatic terminal	12	94%	91%
4	 2-phenyloxirane	 4-(phenyl)-1,3-dioxolan-2-one	Aromatic terminal	24	88%	69%
5	 1,2-Epoxycyclohexane	 4,5 Tetramethylene-1,3-dioxolane-2-one	Six-membered internal	24	<12%	—
6	 1,2-Epoxycyclopentane	 tetrahydro-4H-cyclopenta[d][1,3]dioxol-2-one	Five membered internal	24	~20%	—

have been previously documented, and the data presented in Table 4 align with the existing literature. Although 2-propyloxirane carries a bulkier substituent, the initially lower yield observed with 2-methyloxirane is likely attributed to its higher volatility under solvent-free conditions at 100 °C, resulting in partial loss during the reaction. To validate this, the experiment was repeated with 2-methyloxirane, and by cooling the reaction mixture to 0 °C prior to product extraction, the isolated yield significantly improved to 89%, supporting the volatility-related explanation.

The durability and reusability of the **Ce-TPTC-NH₂** catalyst were assessed through successive cycloaddition reactions of

epoxides and CO₂ under optimized conditions. The catalyst was recovered *via* centrifugation, washed thoroughly with ethyl acetate, and dried at 70 °C overnight. **Ce-TPTC-NH₂** exhibited remarkable durability, retaining ~90% of its catalytic activity even after five cycles while maintaining high selectivity. The stability of parent and reused **Ce-TPTC-NH₂** samples was confirmed using PXRD and HR-TEM analysis. The PXRD patterns after five catalytic cycles showed that the crystallinity of the MOF was retained, with a slight decrease in peak intensity (Fig. S10†). The HRTEM images revealed that the morphology and particle integrity were well preserved, with no visible aggregation, collapse, or structural degradation before and

after catalysis (Fig. S11†). The HRTEM analysis of the as-synthesized **Ce-TPTC-NH₂** MOF revealed a uniform particle morphology with an expected particle size in the range of 1–2 μm , as referred to by dynamic light scattering (DLS) experiment data (Fig. S12†).

However, after five cycles, the conversion efficiency declined to $\sim 85\%$, likely due to partial blockage of active sites. Additionally, complete catalyst recovery was not achieved, potentially due to minor losses during filtration and washing, structural degradation, or partial leaching of active species. To assess the extent of cerium leaching, the post-reaction filtrate was analyzed by microwave plasma-atomic emission spectroscopy (MP-AES). The initial Ce content in the catalyst before catalysis was determined to be 63 ppm in a 100 ppm dispersion, which slightly decreased to 58 ppm after the fifth cycle. This minor decrease indicates negligible Ce leaching ($\sim 7.9\%$), confirming the structural robustness and recyclability of the catalyst under the applied reaction conditions. The catalytic performance of **Ce-TPTC-NH₂** was compared with selected MOF and organocatalyst systems reported in the literature (see Table 3).

Proposed mechanism of CO₂ conversion

The cycloaddition of CO₂ with epoxides to form cyclic carbonates, catalyzed by **Ce-TPTC-NH₂**, follows a plausible synergistic activation mechanism involving Lewis acidic Ce(III) centers and nucleophilic amino ($-\text{NH}_2$) functional groups (Fig. 6). However, activating CO₂ transformation requires significant energy due to the high bond enthalpy of the C=O bond ($+805 \text{ kJ mol}^{-1}$). The catalytic cycle begins with electron-rich amine ($-\text{NH}_2$) group acting as Lewis base, interacting with the carbon atom of CO₂ and stabilizing its acidic nature.

Simultaneously, the Lewis-acidic Ce(III) centers coordinate with the oxygen atom of the epoxide, increasing its electrophilicity. In the second step, the Br[−] anion, generated from TBAB (co-catalyst), then initiates a nucleophilic attack on the activated epoxide, leading to the formation of an alkoxide-metal intermediate. Subsequently, CO₂ insertion into this alkoxide complex promotes intramolecular cyclization, yielding a five-membered cyclic carbonate. In the final step, the bromide ion is released and reintegrated into the catalytic cycle, ensuring continuous turnover of the active Ce(III) species. The cyclic carbonate product detaches from the metal center, preserving the catalyst integrity and allowing for successive reaction cycles with minimal deactivation.^{40,45} This catalytic system demonstrates excellent activity and selectivity in cyclic carbonate synthesis, offering a sustainable and efficient route for CO₂ utilization. Operating under ambient to mild conditions with a reusable catalyst aligns with green chemistry principles, converting CO₂ into valuable chemical products. Integrating CO₂ as a feedstock mitigates greenhouse gas emissions and advances sustainable carbon valorization, paving the way for practical and environmentally benign CO₂ conversion strategies.

Experimental

Materials

Cerium(III) nitrate hexahydrate (Reacton™, 99.5%) was purchased from Alfa Aesar. (3,5-Bis(methoxy carbonyl)phenyl) boronic acid, palladium acetate (Pd(OAc)₂), 2,5-dibromoaniline ($>98\%$), tetrabutyl ammonium bromide (TBAB), and cesium carbonate (Cs₂CO₃) were purchased from Sigma-Aldrich. Dimethyl formamide (DMF) and nitric acid (69%) were purchased from Merck.

Synthetic procedure

Synthesis of 2'-amino-1,1':4',1''-terphenyl-3,5,3',5'-tetracarboxylic acid (TPTC-NH₂). The synthesis was performed following a modified procedure as shown in Scheme 1.⁴⁶ First, tetramethyl 2'-amino-[1,1':4',1''-terphenyl]-3,3'',5,5''-tetracarboxylate (Me₄L-NH₂) was synthesized under nitrogen atmosphere. A mixture of 3,5-bis(methoxy carbonyl)phenylboronic acid (0.238 g, 1 mmol), 2,5-dibromoaniline (0.063 g, 0.25 mmol), Pd(OAc)₂ (0.0015 g, 0.0067 mmol) and Cs₂CO₃ (0.325 g, 1 mmol) was added to a solution of deoxygenated *N,N*-dimethylformamide (8 mL) and water (10 mL) in a 100 mL two neck round bottom flask, which was then refluxed at 105 °C for 12 hours. The reaction was allowed to cool at room temperature, and the greenish-yellow mixture was extracted with ethyl acetate and brine water three times; ethyl acetate was dried over anhydrous Na₂SO₄ and removed under reduced pressure. Further purification of compound Me₄L-NH₂ was done by column chromatography (EtOAc : hexane = 30 : 70 by volume; *R_f*: 0.38), yielding a light-yellow compound (0.286 g, 0.6 mmol). Yield: 64%. ¹H NMR (400 MHz, DMSO-*d*₆), δ = 8.68 (d, 2 H), 8.48 (s, 2H), 8.39 (s, 2H), 7.24 (s, 1H), 7.15 (d, 1H), 7.08 (s, 1H), 3.98 (d, 12H) ppm.

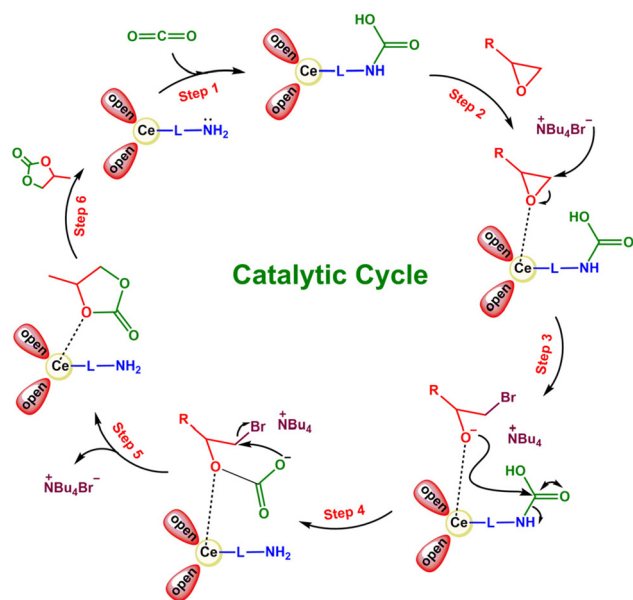


Fig. 6 Catalytic cyclic process of conversion of epoxide into cyclic carbonate.

Tetramethyl 2'-amino-[1,1':4',1''-terphenyl]-3,3'',5,5''-tetra carboxylate (0.286 g, 0.6 mmol) was then suspended in THF (10 mL) for 30 minutes, to which 20 mL of 5.50 M KOH in an aqueous ethanol solution was added. The mixture was stirred under reflux overnight at 65 °C. The reaction was allowed to cool at room temperature and centrifuged to collect the precipitates. The precipitates were then suspended to 10 mL THF, followed by a dropwise addition of dilute HCl until the solution pH reached 2–3. Excess water was added to the mixture to achieve the quick precipitation of a light-yellow solid as the product. The solid was collected by filtration, washed with water, and dried to give TPTC-NH₂ (Fig. S1–S3†). Yield: 93.2%. ¹H NMR (400 MHz, DMSO-D₆): δ = 8.40 (d, *J* = 1.4 Hz, 2H), 8.33 (s, 1H), 8.17 (s, 2H), 7.49 (s, 1H), 7.35 (d, 1H), 7.21 (d, 1H), 3.15 (d, 2H). *m/z* (ESI-MS) [*M* – *H*]: 422.08. Elemental analysis (%) calc.: C, 62.71; H, 3.59; N, 3.32; O, 30.38.; found: C, 62.51; H, 3.89; N, 3.22; O, 30.18.

Synthesis of Ce-TPTC-NH₂ MOF

The synthesis of MOF Ce-TPTC-NH₂ was performed following a modified procedure (Scheme 2).²² A mixture of Ce(NO₃)₃·6H₂O (0.130 g, 0.3 mmol) and TPTC-NH₂ (42 mg, 0.1 mmol) was dissolved separately in DMF (10 mL) and added to a screw-capped vial. Further, two drops of HNO₃ (65%, aq) were added to the mixture. The vial was sealed and placed in a preheated oven at 105 °C for 24 hours. Crystals were obtained after 48 hours and air-dried. Yield: 59% (based on TPTC-NH₂ ligand). The solvent exchange was carried out for three days with fresh acetone every day.

General procedure of catalytic coupling of epoxide and CO₂

Before the catalytic test, Ce-TPTC-NH₂ MOF was activated by heating at 100 °C under vacuum to remove the guest solvent. The reaction was carried out in a stainless-steel high-pressure reactor, where (2 mL, 25.3 mmol) of the epoxide was added along with 0.06 mol% of catalyst and (16 mg, 0.5 mmol) TBAB. The reactor was sealed and purged with 5 bar CO₂. The temperature was maintained at 100 °C under stirring for 24 h. Upon completion, the reaction mixture was cooled to 0 °C, and a small aliquot was taken for catalyst separation *via* centrifugation. The crude product was purified using column chromatography with a mixture of ethyl acetate and hexane. The progress of the reaction was periodically monitored using ¹H and ¹³C nuclear magnetic resonance (NMR) spectroscopy in CDCl₃.

Conclusions

In this study, we have successfully synthesized, crystallized, and characterized a novel amine-functionalized Ce(III) MOF (Ce-TPTC-NH₂) and demonstrated its noteworthy efficiency in the catalytic conversion of CO₂ into value-added cyclic carbonates. Single-crystal X-ray diffraction (SCXRD) confirmed its well-defined 3D crystalline structure, while spectroscopic

and adsorption studies validated the presence of accessible Lewis-acidic Ce(III) sites and uncoordinated (–NH₂) groups. The TPD studies further validated the coexistence of both acidic and basic sites, which is pivotal in enhancing catalytic performance. The Ce-TPTC-NH₂ MOF exhibited remarkable stability under catalytic conditions, achieving nearly quantitative conversion (98%). Furthermore, the catalyst demonstrated excellent stability and reusability, retaining ~90% of its activity after five consecutive cycles as confirmed by PXRD, HR-TEM, and MP-AES analysis. The cooperative interaction between the Lewis acidic cerium sites and the nucleophilic amine functionalities significantly enhances CO₂ adsorption and activation, effectively overcoming the intrinsic thermodynamic and kinetic barriers associated with CO₂ transformation. This synergistic effect is further validated by the reduced catalytic performance observed with the Ce-TPTC catalyst lacking the –NH₂ functionality. The mechanistic insights gained from this study provide a deeper understanding of structure–activity relationships in MOF-based catalysts for CO₂ fixation. Overall, our work contributes to the advancement of metal–organic frameworks in catalytic CO₂ conversion and presents a promising strategy for sustainable carbon utilization, aligning with green chemistry principles for efficient CO₂ valorization. Given the redox-active nature of cerium, Ce-TPTC-NH₂ holds potential for photocatalysis, offering new avenues for light-driven CO₂ conversion and sustainable transformations.

Author contributions

Yogesh Kumar – original draft, methodology, investigation, formal analysis, and data curation. Rishukumar Panday – single crystal data analysis, investigation, and formal analysis. Shaibal Banerjee – writing – review and editing, validation, supervision, resources, and conceptualization.

Conflicts of interest

There are no conflicts to declare.

Data availability

The data supporting this article have been included as part of the ESI.†

Acknowledgements

This study was financially supported by the Defence Research and Development Organisation (DRDO). The author thanks Ramamoorthy Boomishankar, Department of Chemistry, Indian Institute of Science Education and Research, Pune, for providing crystal data support.

References

- 1 M. Ding, R. W. Flaig, H.-L. Jiang and O. M. Yaghi, *Chem. Soc. Rev.*, 2019, **48**, 2783–2828.
- 2 K. Sumida, D. L. Rogow, J. A. Mason, T. M. McDonald, E. D. Bloch, Z. R. Herm, T.-H. Bae and J. R. Long, *Chem. Rev.*, 2012, **112**, 724–781.
- 3 T. Jose, Y. Hwang, D.-W. Kim, M.-I. Kim and D.-W. Park, *Catal. Today*, 2015, **245**, 61–67.
- 4 W. N. Sit, S. M. Ng, K. Y. Kwong and C. P. Lau, *J. Org. Chem.*, 2005, **70**, 8583–8586.
- 5 F. Heshmatpour and R. Abazari, *RSC Adv.*, 2014, **4**, 55815–55826.
- 6 O. M. Yaghi, M. O'Keeffe, N. W. Ockwig, H. K. Chae, M. Eddaoudi and J. Kim, *Nature*, 2003, **423**, 705–714.
- 7 H. Furukawa, K. E. Cordova, M. O'Keeffe and O. M. Yaghi, *Science*, 2013, **341**, 1230444.
- 8 M. J. Kalmutzki, N. Hanikel and O. M. Yaghi, *Sci. Adv.*, 2018, **4**, eaat9180.
- 9 W. Lu, Z. Wei, Z.-Y. Gu, T.-F. Liu, J. Park, J. Park, J. Tian, M. Zhang, Q. Zhang and T. Gentle III, *Chem. Soc. Rev.*, 2014, **43**, 5561–5593.
- 10 V. Guillermin, H. Jiang, D. Alezi, N. Alsadun and M. Eddaoudi, *Adv. Mater.*, 2024, 2414153.
- 11 F. Vermoortele, R. Ameloot, A. Vimont, C. Serre and D. De Vos, *Chem. Commun.*, 2011, **47**, 1521–1523.
- 12 F. Vermoortele, M. Vandichel, B. Van de Voorde, R. Ameloot, M. Waroquier, V. Van Speybroeck and D. E. De Vos, *Angew. Chem., Int. Ed.*, 2012, **51**, 4887–4890.
- 13 H. Molavi, *Coord. Chem. Rev.*, 2025, **527**, 216405.
- 14 G. Ji, L. Zhao, J. Wei, J. Cai, C. He, Z. Du, W. Cai and C. Duan, *Angew. Chem., Int. Ed.*, 2022, **61**, e202114490.
- 15 K. Hendrickx, J. J. Joos, A. De Vos, D. Poelman, P. F. Smet, V. Van Speybroeck, P. Van Der Voort and K. Lejaeghere, *Inorg. Chem.*, 2018, **57**, 5463–5474.
- 16 F. Nouar, M. I. Breeze, B. C. Campo, A. Vimont, G. Clet, M. Daturi, T. Devic, R. I. Walton and C. Serre, *Chem. Commun.*, 2015, **51**, 14458–14461.
- 17 Y. Zhang, H. Chen, Y. Pan, X. Zeng, X. Jiang, Z. Long and X. Hou, *Chem. Commun.*, 2019, **55**, 13959–13962.
- 18 S. Dai, E. Montero-Lanzuela, A. Tissot, H. G. Baldoví, H. García, S. Navalón and C. Serre, *Chem. Sci.*, 2023, **14**, 3451–3461.
- 19 X.-P. Wu, L. Gagliardi and D. G. Truhlar, *J. Am. Chem. Soc.*, 2018, **140**, 7904–7912.
- 20 X. Han and M. Poliakoff, *Chem. Soc. Rev.*, 2012, **41**, 1428–1436.
- 21 D. Kim, D. W. Kim, O. Buyukcakir, M. K. Kim, K. Polychronopoulou and A. Coskun, *Adv. Funct. Mater.*, 2017, **27**, 1700706.
- 22 A. Ma, F. Ke, J. Jiang, Q. Yuan, Z. Luo, J. Liu and A. Kumar, *CrystEngComm*, 2017, **19**, 2172–2177.
- 23 M. Lammert, M. T. Wharmby, S. Smolders, B. Bueken, A. Lieb, K. A. Lomachenko, D. De Vos and N. Stock, *Chem. Commun.*, 2015, **51**, 12578–12581.
- 24 Y. Hu, R. Abazari, S. Sanati, M. Nadafan, C. L. Carpenter-Warren, A. M. Slawin, Y. Zhou and A. M. Kirillov, *ACS Appl. Mater. Interfaces*, 2023, **15**, 37300–37311.
- 25 R. Abazari, S. Sanati, A. Morsali, A. M. Kirillov, A. M. Slawin and C. L. Carpenter-Warren, *Inorg. Chem.*, 2021, **60**, 2056–2067.
- 26 J. F. Kurisingal, Y. Rachuri, Y. Gu, R. K. Chitumalla, S. Vuppala, J. Jang, K. K. Bisht, E. Suresh and D.-W. Park, *ACS Sustainable Chem. Eng.*, 2020, **8**, 10822–10832.
- 27 S. Payra and S. Roy, *J. Phys. Chem. C*, 2021, **125**, 8497–8507.
- 28 J. X. Gu, H. Chen, Y. Ren, Z. G. Gu, G. Li, W. J. Xu, X. Y. Yang, J. X. Wen, J. T. Wu and H. G. Jin, *ChemSusChem*, 2022, **15**, e202102368.
- 29 J. Senith Ravishan Fernando, S. S. Asaithambi and S. Maruti Chavan, *ChemPlusChem*, 2024, **89**, e202400107.
- 30 Q. Sun, H. Gao, M. Xiao, T. Sema and Z. Liang, *Environ. Sci. Technol.*, 2024, **58**, 10052–10059.
- 31 P. Gabrielli, M. Gazzani and M. Mazzotti, *Ind. Eng. Chem. Res.*, 2020, **59**, 7033–7045.
- 32 C. C. Truong and D. K. Mishra, *J. CO₂ Util.*, 2020, **41**, 101252.
- 33 X.-H. Ji, N.-N. Zhu, J.-G. Ma and P. Cheng, *Dalton Trans.*, 2018, **47**, 1768–1771.
- 34 J. Cai, H. Wang, H. Wang, X. Duan, Z. Wang, Y. Cui, Y. Yang, B. Chen and G. Qian, *RSC Adv.*, 2015, **5**, 77417–77422.
- 35 W.-M. Liao, M.-J. Wei, J.-T. Mo, P.-Y. Fu, Y.-N. Fan, M. Pan and C.-Y. Su, *Dalton Trans.*, 2019, **48**, 4489–4494.
- 36 S. Yadav, N. Beniwal, G. Singh, P. Rekha and L. Singh, *ACS Appl. Eng. Mater.*, 2024, **2**, 2946–2961.
- 37 L. Chen, T. V. Janssens, M. Skoglundh and H. Grönbeck, *Top. Catal.*, 2019, **62**, 93–99.
- 38 A. Bavykina, N. Kolobov, I. S. Khan, J. A. Bau, A. Ramirez and J. Gascon, *Chem. Rev.*, 2020, **120**, 8468–8535.
- 39 Q. Yang, C. C. Yang, C. H. Lin and H. L. Jiang, *Angew. Chem.*, 2019, **131**, 3549–3553.
- 40 W.-L. Bao, J. Kuai, H.-Y. Gao, M.-Q. Zheng, Z.-H. Sun, M.-Y. He, Q. Chen and Z.-H. Zhang, *Dalton Trans.*, 2024, **53**, 6215–6223.
- 41 C.-Y. Gao, J. Ai, H.-R. Tian, D. Wu and Z.-M. Sun, *Chem. Commun.*, 2017, **53**, 1293–1296.
- 42 S. K. Das, S. Chatterjee, S. Bhunia, A. Mondal, P. Mitra, V. Kumari, A. Pradhan and A. Bhaumik, *Dalton Trans.*, 2017, **46**, 13783–13792.
- 43 D. H. Le, R. P. Loughan, A. Gladysiak, N. Rampal, I. A. Brooks, A.-H. A. Park, D. Fairen-Jimenez and K. C. Stylianou, *J. Mater. Chem. A*, 2022, **10**, 1442–1450.
- 44 J. Liang, R.-P. Chen, X.-Y. Wang, T.-T. Liu, X.-S. Wang, Y.-B. Huang and R. Cao, *Chem. Sci.*, 2017, **8**, 1570–1575.
- 45 Z.-Q. Li, Y.-Y. Zhang, Y.-J. Zheng, B. Li and G.-P. Wu, *J. Org. Chem.*, 2022, **87**, 3145–3155.
- 46 D. De, T. K. Pal, S. Neogi, S. Senthilkumar, D. Das, S. S. Gupta and P. K. Bharadwaj, *Chem. – Eur. J.*, 2016, **22**, 3387–3396.